iomac
International Operational Modal Analysis Conference

11th International Operational Modal Analysis Conference

20 - 23 May 2025 | Rennes, France

# Optimal sensor placement of FBGs based on the effective independence method for OMA of a Vierendeel truss bridge

*Dimitrios Anastasopoulos* [1], *Eleni N. Chatzi* [2], *Geert Lombaert* [1] *and Edwin P. B. Reynders* [1]

[1] Department of Civil Engineering, KU Leuven, Leuven, Belgium. E-mail: dimitrios.anastasopoulos@kuleuven.be

[2] Department of Civil, Environmental and Geomatic Engineering, ETH Zurich, Zurich, Switzerland.

**ABSTRACT**

Optimal Sensor Placement (OSP) is an optimization problem aimed at identifying sensor positions that maximize the value of information obtained from the employed sensor configuration. The Fisher Information Matrix (FIM) has been widely explored for the development of OSP methods for civil engineering structures. The Effective Independence (EfI) method complements the FIM in OSP by providing information on the contribution of each candidate sensor to the determinant of the FIM, allowing the least important sensor to be excluded during each iteration. By repeating this process, an optimal setup containing the desired number of sensors can be obtained. The FIM and EfI methods have demonstrated their effectiveness for optimal placement of accelerometers in both laboratory and full-scale structures. However, their application to fiber-optic sensors, such as Fiber-Bragg Gratings (FBG), has been limited. In this study, these methods are applied to optimize the placement of FBG sensors for strain-based Operational Modal Analysis (OMA) of a Vierendeel truss bridge. The optimization process aims to identify the sensor configuration that yields the most information on the strain mode shapes of a set of considered modes. Starting with candidate locations determined by a user-specified strain threshold, the methodology iteratively refines the sensor layout to achieve an optimized configuration of 80 sensors—matching the acquisition system's capacity. A calibrated Finite Element model of the bridge is used to determine the candidate locations, ensuring a robust optimization process. This study highlights the potential of combining FIM and EfI for advancing OSP techniques in FBG networks for strain-based SHM.

*Keywords: Optimal Sensor Placement, Fiber-Bragg Gratings, Operational Modal Analysis, Fisher Information Matrix, Effective Independence*

## 1. INTRODUCTION

Strain-based monitoring, encompassing both static and dynamic approaches, is a valuable tool for Structural Health Monitoring (SHM) of civil infrastructure. It allows early-stage damage detection due to the more significant effect of damage on the strain field in its immediate vicinity [1]. Fiber-optic sensors, such as Fiber-Bragg Gratings (FBGs), can measure strains with high accuracy and precision, making them extensively used for monitoring purposes [2, 3]. Given the virtually infinite number of locations where small-scale damage might occur in a civil structure, some a priori knowledge of the most damage-prone areas is required to strategically place sensors in these critical locations.

This is one of the reasons that has prompted the development of Optimal Sensor Placement (OSP) methods, which aim to maximize the information obtained from a monitoring system while minimizing costs [3, 4]. Some of the most widely used methods include the Modal Kinetic Energy (MKE), the Information Entropy Index (IEI), and the Effective Independence (EfI) method [4, 5]. Among these, the EfI method is particularly influential and is adopted in this study for OSP of long-gauge FBGs on a historical Vierendeel truss steel railway bridge, the M2.17 bridge.

The M2.17 (Fig. 1) is a 92.54 m long Vierendeel truss railway bridge located in the city of Mechelen in Belgium. It was constructed in 1935 and today it is classified as a heritage structure. The bridge has a two-track deck, and the western track is operational, which means that trains currently run only from South to North. (Fig. 2). The bridge rests on four supports, which directly sit on concrete abutments. The supports were designed to act as hinges on the south side and as rollers on the north side.

**Figure 1:** East (left) and south (right) view of the M2.17 railway bridge.

The bridge has already been monitored for more than two years with a dense grid of long-gauge FBGs. The FBGs measure the dynamic deformations of the bridge, which are used to obtain its modal characteristics by means of strain-based Operational Modal Analysis (OMA) [2]. However, the current FBG setup has not been formally evaluated through a formal OSP procedure. Its primary purpose has been to monitor a priori selected locations known to be prone to fatigue damage and brittle failure, particularly due to the critical effect of temperature on the bridge's load-carrying capacity. This is a result of the ductile-to-brittle transition of its structural steel at freezing temperatures [2, 6]. In this paper, an OSP approach based on the EfI method and the Fisher Information Matrix (FIM) is adopted, incorporating prior knowledge of fatigue-prone locations to assess the effectiveness of the current FBG setup.

The adopted EfI-based methodology for the OSP of long-gauge FBGs is presented in Section 2. The current monitoring setup of the M2.17 bridge is detailed in Section 3. A Finite Element model of the bridge, used to determine its modal characteristics and assess the optimized FBG setup, is introduced in Section 4. The results of the OSP, along with the process of optimizing the FBG setup in comparison to the existing configuration, are provided in Section 5. Finally, concluding remarks are given in Section 6.

## 2. METHODOLOGY

In this section, a brief summary of the basic concepts of the Fisher Information Matrix (FIM) and the Effective Independence (EfI) method is provided.

### 2.1. Fisher Information Matrix

The FIM is a classical metric that is used for evaluating experimental designs. It represents the effectiveness of an experimental setup in estimating unknown system parameters [5], which renders FIM a widely used concept for OSP. In its simplest form, assuming a linear relationship between the unknown system parameters and the measured data, the FIM is obtained as [5]:

$$\mathbf{F} = \mathbf{S}^{\mathbf{T}}\boldsymbol{\Sigma}^{-1}\mathbf{S} \tag{1}$$

where $\mathbf{S} \in \mathbb{R}^{n\times p}$ is a sensitivity matrix, characterizing the linear relationship between the unknown system parameters $\boldsymbol{\theta} \in \mathbb{R}^p$ and the measured data $\mathbf{x} \in \mathbb{R}^n$ as:

$$\mathbf{x} = \mathbf{S}\boldsymbol{\theta} + \boldsymbol{\eta} \tag{2}$$

where $\boldsymbol{\eta} \in \mathbb{R}^n$ is the error vector, accounting for the incompleteness of the linearity assumption due to measurement noise. $\boldsymbol{\Sigma}$ is the error covariance matrix.

For modal identification, the measured time histories can be considered as the measured data, in this case the strain time histories $\boldsymbol{\varepsilon}(\mathbf{t})$ recorded by the FBGs, and the modal coordinates $\mathbf{q}(\mathbf{t})$ as the unknown parameters. The linear relationship between the measured time series and the modal coordinates is $\boldsymbol{\varepsilon}(\mathbf{t}) = \boldsymbol{\Psi}\mathbf{q}(\mathbf{t})$, where $\boldsymbol{\Psi}$ is the strain mode shape matrix, with columns representing each mode's strain mode shape as obtained at the locations of the FBG sensors. Thus, the sensitivity matrix is $\mathbf{S} = \boldsymbol{\Psi}$.

Since identical sensors with the same noise characteristics are used, and potential modeling errors that might induce correlations between observations (particularly when sensors are in close proximity [7]) can be mitigated by pre-selecting a subset of candidate sensor locations to avoid placing sensors too close to each other, the covariance matrix $\boldsymbol{\Sigma}$ is assumed to have uniform variance $\boldsymbol{\sigma^2}$, leading to $\boldsymbol{\Sigma} = \boldsymbol{\sigma^2}\mathbf{I}$. Furthermore, since the variance is uniform, it only influences the scaling of the Effective Independence (EfI). To simplify the analysis and improve computational efficiency, the variance is set as $\sigma^2 = 1$. Consequently, the FIM is given by:

$$\mathbf{F} = \boldsymbol{\Psi}^{\mathbf{T}}\boldsymbol{\Psi} \tag{3}$$

### 2.2. Effective Independence

An optimal sensor layout can be determined by starting with an initial set of potential sensor locations, which may include all degrees of freedom in the system, and iteratively eliminating sensors until the desired number remains. This approach, known as the sequential deletion method or backward sequential placement algorithm [4, 5], removes sensors one by one based on an optimization criterion. Typically, the objective function to be minimized is the determinant of the Fisher Information Matrix (FIM). A widely used criterion for sensor removal is the Effective Independence (EfI), defined as:

$$e_i = 1 - \frac{\det(\mathbf{F}_{\text{-}i})}{\det(\mathbf{F})} \tag{4}$$

where $e_i$ the EfI of sensor $i$, and $\det(\mathbf{F})$ and $\det(\mathbf{F}_{\text{-}i})$ denote the determinant of the FIM before and after removing sensor $i$ (corresponding to row $i$ in $\mathbf{F}$), respectively. The EfI values range from zero to one, with lower values indicating sensors that contribute less to the determinant of the FIM and, consequently, to the linear independence of the mode shapes [4]. During each sequential deletion step, the sensor with the lowest EfI is removed, ensuring that the remaining sensors maximize the information gain. It should be acknowledged that the space of possible sensor placements is discrete and combinatorial, often leading to a non-convex solution space. In such cases, greedy or sequential removal methods can get stuck in local optima rather than finding the global optimum.

Having established the fundamental FIM case (Eq. 3), and in order to calculate the EfI of a sensor $i$, the FIM after removing the sensor, $\det(\mathbf{F}_{\text{-}i})$ needs to be calculated:

$$\mathbf{F}_{\text{-}i} = \mathbf{F} - \boldsymbol{\psi}_i\boldsymbol{\psi}_i^{\mathbf{T}} \tag{5}$$

where $\boldsymbol{\psi}_i^{\mathbf{T}}$ is a row vector representing the removed $i$-th row of $\boldsymbol{\Psi}$. Substituting Eq. 5 into Eq. 4:

$$e_i = 1 - \frac{\det(\mathbf{F} - \boldsymbol{\psi}_i \boldsymbol{\psi}_i^{\mathbf{T}})}{\det(\mathbf{F})} \tag{6}$$

The numerator in Eq. 6 is a special case of the matrix determinant lemma, which applies when a matrix is updated by adding a rank-1 matrix. The lemma states that for an invertible matrix $\mathbf{A}$ and a vector $\mathbf{v}$:

$$\det(\mathbf{A} + \mathbf{v}\mathbf{v}^{\mathrm{T}}) = \det(\mathbf{A}) \cdot \left(1 + \mathbf{v}^{\mathrm{T}} \mathbf{A}^{-1} \mathbf{v}\right) \tag{7}$$

Hence, Eq. 6 can be written as:

$$e_i = \boldsymbol{\psi}_i^{\mathbf{T}} \mathbf{F}^{-\mathbf{1}} \boldsymbol{\psi}_i \tag{8}$$

The EfI vector, which consists of the EfI values for all sensors, is then obtained as [5]:

$$\mathbf{e} = \mathrm{diag}(\boldsymbol{\Psi} \mathbf{F}^{-\mathbf{1}} \boldsymbol{\Psi}^{\mathbf{T}}) \tag{9}$$

## 3. MONITORING SETUP

The M2.17 bridge has been continuously monitored since October 2022. The SHM system is based on the monitoring of long-gauge strains or macrostrains at 64 critical locations with FBG sensors. The surface temperature of the bridge is also monitored at five locations, as well as its vertical acceleration on two columns. An overview of the monitoring setup is shown in Fig. 2.

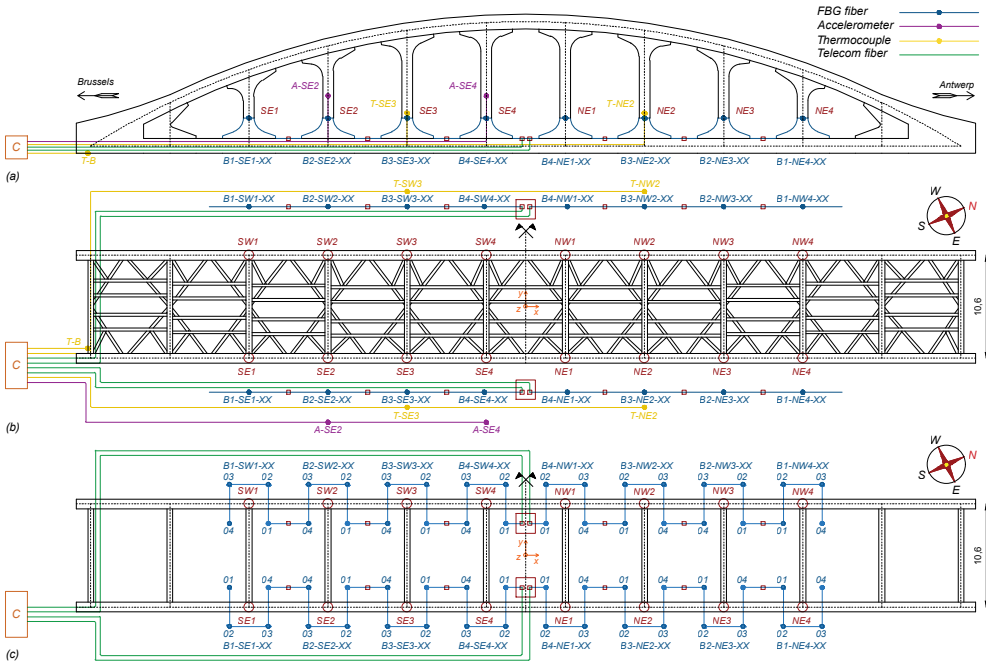


**Figure 2:** Monitoring setup of the M2.17 bridge. (a) Side view; (b) and (c) top view of the bridge deck, with the complete sensor layout and the detailed FBG layout, respectively. B*i*-*ORN*-*XX* are the FBG fibers. T-*ORN* and T-*B* are the temperature sensors on the columns and underneath the deck, respectively. A-*ORN* are the uniaxial accelerometers. C is the cabinet containing the acquisition systems and the measurement PC.

The tapered cross-sections at the ends of the columns (Fig. 3) cause high stress concentrations at the start of the tapered zones, which renders these locations more prone to fatigue damage and brittle failure. To address this, the tapered zones at the bottom part of every column are monitored with four FBGs (Fig. 3).

Due to their proximity to the overhead electrical lines of the railway, the top tapered zones of the columns could not be accessed; hence, they are not monitored, which potentially leads to a sub-optimal FBG setup.

Sixty-four FBGs are required for the bottom tapered zones, which are inscribed in 16 fibers, each containing 4 sensors. The FBGs are pretensioned and then firmly fixed in custom clamping blocks (Fig. 3c). They measure the average longitudinal strain between two clamping blocks over a gauge length of 85 cm. Since FBGs are also sensitive to thermal strain, they are covered with thermal insulation (Fig. 3b) to minimize the effect of fast temperature fluctuations on the measurements.

The fibers are divided into four batches (B1-B4) based on the nominal wavelength of the inscribed FBGs. The columns are divided into four groups according to their orientation. Each four-column group includes one fiber from each batch, which are connected in series in ascending wavelength order (Fig. 2).

Every hour, twenty minutes of strain data are recorded at a sampling rate of 1000 Hz, starting at the hour mark and up to twenty minutes past the hour. The bridge temperature is measured at five locations using standard type T thermocouples installed on four columns and under the bridge deck (Fig. 2). The mean temperature of each thermocouple record over the 20 min measurement period is stored.

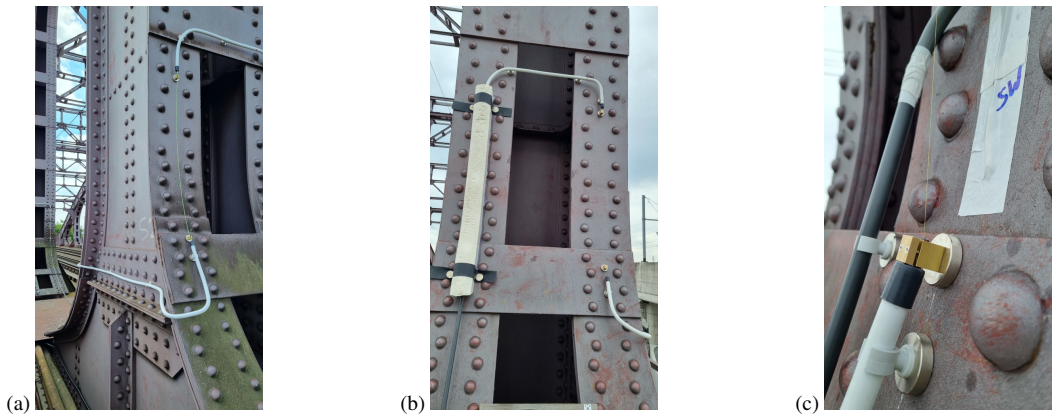

**Figure 3:** Installation of the FBG fibers: (a) side view; (b) front view of the protective tubes and the FBG fiber before covering (right flange) and after covering with thermal insulation (left flange); (c) clamping block (brass) for connecting a fiber on a column.

## 4. FINITE ELEMENT MODEL

A three-dimensional (3D) linear elastic finite element (FE) model of the bridge is constructed (Fig. 4) using the MATLAB toolbox Stabil 3.1 [8]. The FE model serves to provide a physical interpretation of the experimental results and to obtain an optimized sensor setup.

The bridge is modeled using Timoshenko beam elements with uniform cross-sections. The columns are also modeled with beam elements but cross-sections with three different widths are used to account for the tapered column ends. The material properties assigned to structural steel are: $E_\mathrm{s} = 201\,\mathrm{GPa}$ for the Young's modulus, $\rho_\mathrm{s} = 7850\,\mathrm{kg/m^3}$ for the density and $\nu_\mathrm{s} = 0.3$ for the Poisson's ratio. Initially, the boundary conditions correspond to those of a simply supported bridge, i.e., the south end supports act as hinges and the north end as rollers. A detailed description of the FE model is given in [2].

### 4.1. Model calibration

The model is calibrated based on the results of a detailed acceleration-based OMA [2], which was performed before the installation of the permanent monitoring system. The first nine modes are considered in the calibration process, which match with the modes that were identified by the OMA.

To improve the accuracy of the model, the steel's density is increased by $15\%$ to account for the additional mass of the non-structural components. Moreover, the boundary conditions are modified so that the

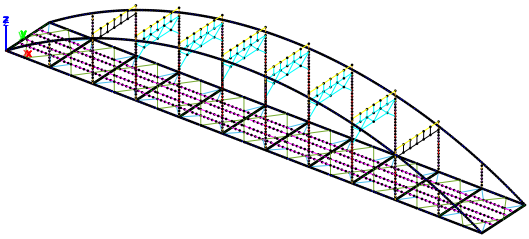

**Figure 4:** 3D view of the FE model of the M2.17 bridge in Stabil, with different colors representing various structural elements and sections.

modal displacements of the model's supports can match the experimentally identified ones. Small modal displacements were observed along all directions at the location of the pins, as well as at the vertical and transversal direction of the rollers. This indicates that the dynamic boundary conditions do not correspond to perfect pins and rollers. Hence, uniaxial translation springs are introduced at the supports.

The same spring stiffness is assumed for the lateral ($K_{\mathrm{yy}}$) and vertical translations ($K_{\mathrm{zz}}$) of both the pins and the rollers, as well as for the horizontal translation ($K_{\mathrm{xx,P}}$) of the pins. In general, a good agreement is obtained between the measured and the numerical results for the spring stiffness constants $K_{\mathrm{xx,P}} = K_{\mathrm{yy}} = K_{\mathrm{zz}} = 2.9 \cdot 10^9\,\mathrm{N/m}$, and a mass increase of $15\%$. The horizontal displacement of the rollers is also restrained to account for the dynamic friction forces with a spring stiffness of $K_{\mathrm{xx,R}} = 2 \cdot 10^7\,\mathrm{N/m}$.

After calibrating the model, the agreement between numerical and experimental modal characteristics is high, with the relative error of natural frequencies below $2.5\%$. In addition, the MAC (Modal Assurance Criterion) values between the experimental and the numerical displacement mode shapes vary between 0.91 and 0.99, while the MAC values between the experimental and the numerical strain mode shapes between 0.85 and 0.98. The natural frequencies and the displacement mode shapes of the first three modes that are obtained from the calibrated FE model of the M2.17 bridge are displayed in Fig. 5.

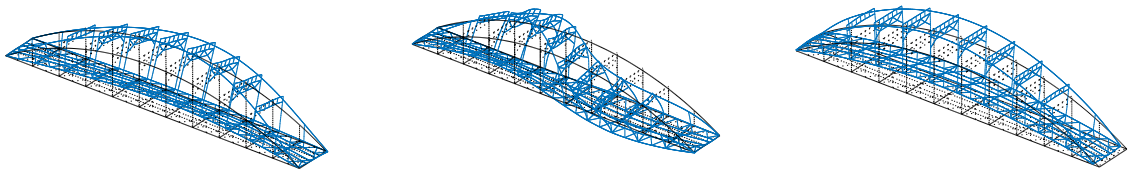

(a) $f_1^{\mathrm{fem}} = 1.31\,\mathrm{Hz}$ (L1) (b) $f_2^{\mathrm{fem}} = 2.73\,\mathrm{Hz}$ (L2) (c) $f_3^{\mathrm{fem}} = 3.06\,\mathrm{Hz}$ (B1)

**Figure 5:** Natural frequencies $f_j^{\mathrm{fem}}$ and displacement mode shapes $\boldsymbol{\phi}_j^{\mathrm{fem}}$ (3D view) of the first three modes of the M2.17 bridge as obtained from the calibrated Stabil FE model.

### 4.2. Strain mode shapes

The numerical strain mode shapes are obtained through the following process. First, the internal modal forces induced by the modal displacements of each mode $j$ are extracted at the FE model nodes $i$. These nodes correspond to the geometric centers of the cross-sections (Fig. 6), where the clamping blocks are attached (Figs. 3 and 6). Since the columns are subjected to a combination of axial loading and biaxial bending, the longitudinal (axial) strains at the clamping blocks can be directly derived from the internal modal forces using Timoshenko beam theory. Therefore, the axial modal strains $\boldsymbol{\psi}_{j,i}^{\mathrm{fem}} \in \mathbb{R}^{4\times 1}$ that correspond to the clamping block positions, are computed for each mode $j$ and node $i$ as:

$$\boldsymbol{\psi}_{j,i}^{\mathrm{fem}} = \frac{N_{j,i}}{A_{\mathrm{c}} E_{\mathrm{s}}} \pm \frac{M_{j,i}^{\mathrm{zz}} y_{\mathrm{c}}}{I_{\mathrm{zz}} E_{\mathrm{s}}} \pm \frac{M_{j,i}^{\mathrm{yy}} z_{\mathrm{c}}}{I_{\mathrm{yy}} E_{\mathrm{s}}} \tag{10}$$

where $N_{j,i}$ is the axial force and $M_{j,i}^{zz}$, $M_{j,i}^{yy}$ are the bending moments around the weak and the strong axis, respectively. $A_c$ is the cross-section area, $I_{zz}$, $I_{yy}$ are the moments of inertia around the weak and the strong axis and $y_c$, $z_c$ the perpendicular distances from the neutral axis in y- and z-direction Fig. 6. Since the FBGs measure the average strain between two clamping blocks, the numerical modal strains are obtained as the average of the point modal strains at the two clamping blocks supporting each FBG.

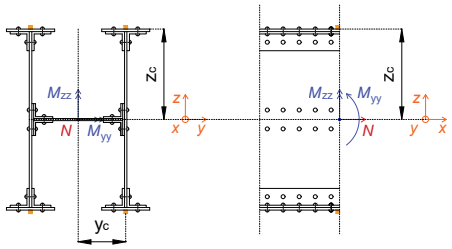


**Figure 6:** Internal axial and bending forces at a typical column cross-section. The orange cubes represent the clamping blocks that are used to attach the FBG fibers on the columns.

In addition to the currently monitored locations, numerical strain mode shapes are also extracted at the top tapered zones of the columns, which could not be instrumented due to their proximity to electrical lines. Other critical regions with high-amplitude modal strains, essential for mode identification, include the midpoints of the arches and girders (modes 1 and 3 in Fig.5b), as well as locations where antisymmetric modes, such as mode 2 in Fig.5b, exhibit maximum modal displacements.

To reduce computational effort, the sensor optimization process begins by selecting a subset of potential locations for attaching FBGs. FBGs can be installed at any location that allows for longitudinal long-gauge strain measurements, such as along the columns. The selected locations are chosen based on their significant contribution to the strain mode shapes, for example the midpoints of the arches, and their relevance for damage detection. In particular, areas with high stress concentrations that are prone to fatigue damage, such as the tapered zones of the columns, are prioritized.

## 5. OPTIMAL FBG PLACEMENT

The first nine eigenmodes are used as input for the FBG sensor placement. The number of original FBG candidate locations is $N_{s,0} = 176$, which means that the matrix of original strain mode shapes $\mathbf{\Psi}_0$ has a size of $176 \times 9$. In Fig. 7a, the candidate FBG locations are indicated. Each location corresponds to a cross-section, where up to 4 FBGs can potentially by attached, as shown in Fig. 6.

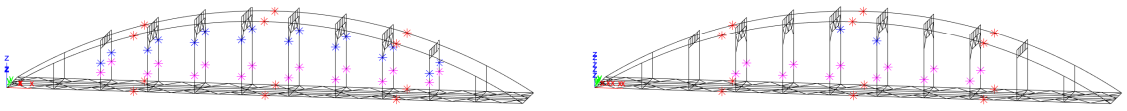

(a) (b)

**Figure 7:** View of the of the M2.17 bridge, showing (a) candidate FBG locations, and (b) the FBG locations after optimization. The stars indicate cross-sections where up to four FBGs can be attached: magenta for the bottom tapered zone, blue for the top, and red for the midpoints, the 1/3 and 2/3 positions along the arches and girders.

For each sensor setup, the FIM (Eq. 3) and EfI (Eq. 9) are computed. The objective is to determine an optimized configuration with $N_{s,OPT} = 80$ FBGs, the maximum number of sensors the acquisition system can handle under ambient conditions. A sequential deletion procedure is employed, where, in each iteration, the sensor with the lowest EfI is removed until the desired number of sensors is reached. A discretized plot with the EfI of each sensor for each iteration is shown in Fig. 8. It can be seen that the EfI is progressively increasing for the arch and girder, as well as the bottom tapered zones FBGs, highlighting the importance of these sensors for modal identification. The optimized setup is shown in Fig. 7b, where all sections where at least one FBG is required are marked.

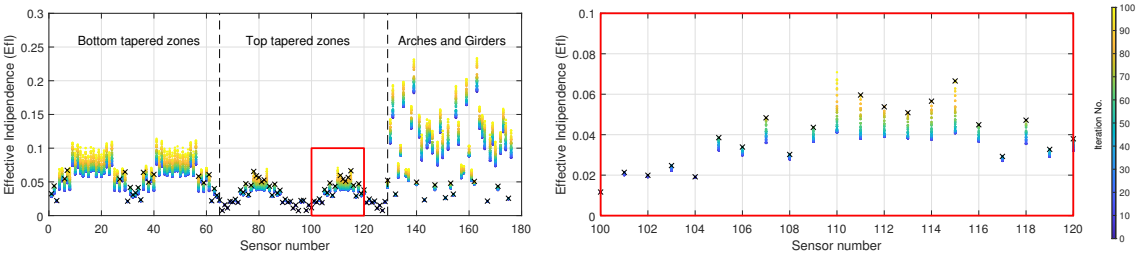


**Figure 8:** (a) Effective Independence (EfI) values obtained at each iteration during the sequential deletion process, continuing until the optimal setup for 80 FBGs is reached. (b) Zoomed-in view of the sensor range from 100 to 120. The $\times$ markers indicate sensors that were removed due to having the lowest EfI in a given iteration.

Notably, only two FBGs are required for the upper tapered zones in columns SW4 and NE1, while most of the sensors in the arches, girders, and bottom tapered zones are retained. Additionally, the FBGs located at the tapered zones of the shortest columns are found to be redundant and thus, removed by the algorithm. As an example, the strain mode shape of the first lateral mode is given in Fig. 9, before and after optimization. The discrete points correspond to the modal strains, as obtained from each FBG.

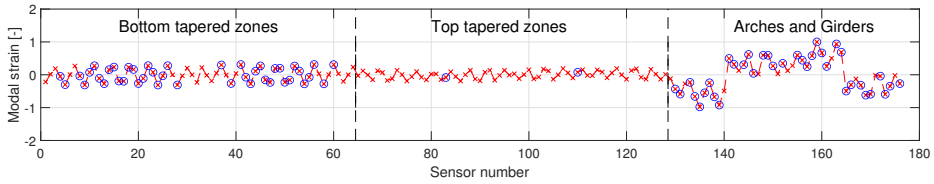


**Figure 9:** Strain mode shape of the first lateral bending mode (Fig. 5a), before (red marks) and after (blue circles) sensor optimization. Each discrete point corresponds to the modal strain obtained by an FBG sensor.

The efficiency of the obtained FBG setup is assessed using the Modal Assurance Criterion (MAC). After each iteration, the auto-MAC is calculated for the numerical strain mode shapes to verify the linear independence of the considered modes. In Figs. 10a and 10b, the auto-MAC values are given for $N_{\mathrm{s},0} = 176$ FBGs and $N_{\mathrm{s,OPT}} = 80$ FBGs, respectively. It is observed that most of the non-diagonal values remain close to zero, while the linear dependence between some of the modes, such as L2 and L4 is reduced with the optimized setup. This result validates the suitability of the optimized setup for OMA.

A scalar index, termed information entropy index (IEI), is employed to quantify the uncertainty in parameter estimation [4]. The IEI is defined as:

$$\mathrm{IEI} = \sqrt{\det(\mathbf{F_0})/\det(\mathbf{F})} \tag{11}$$

where $\mathbf{F_0}$ the reference FIM for $N_{\mathrm{s},0} = 176$ FBGs. The IEI after every sequential deletion is shown in Fig. 10c. An increase in IEI indicates a sensor setup that provides less information about the system and thus, higher uncertainty in parameter estimation. Although IEI increases as sensors are removed, signalling a reduced information value, the modes remain orthogonal (Fig. 10b). This confirms that a high-information-value setup is still achieved, largely due to the extensive number of sensors in the optimized configuration.

## 6. CONCLUSIONS

The Effective Independence method is employed in this paper for the optimal sensor placement (OSP) of long-gauge FBGs on a Vierendeel truss railway bridge. The method is modified to optimize a user-selected subset of sensor locations, rather than considering all potential placements, thereby enhancing computational efficiency. The results show that this approach successfully identifies an optimized sensor configuration, as validated by the auto-MAC, which confirms the linear independence of the mode

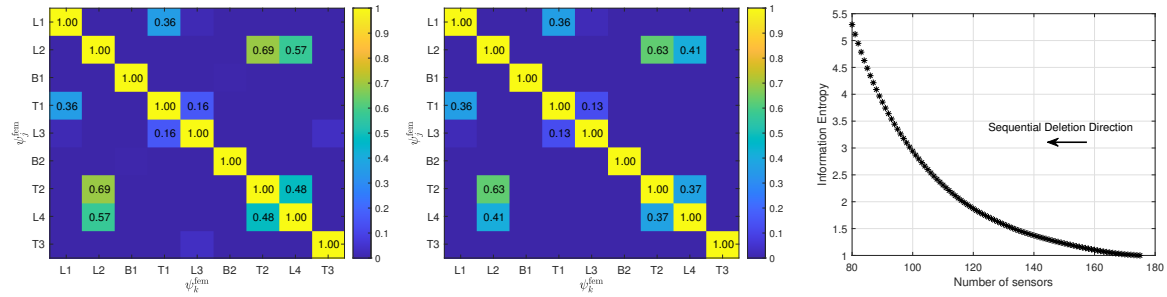


**Figure 10:** Auto-MAC between the numerical strain modes shapes, as obtained for (a) $N_{\mathrm{s},0} = 176$ FBGs, and (b) $N_{\mathrm{s,OPT}} = 80$ FBGs. (c) Information Entropy Index as obtained during the sequential deletion of FBGs.

shapes, even with an increase in the Information Entropy Index. The proposed method assumes that the covariance matrix is the identity matrix. Future work will extend this approach into a stochastic framework to account for uncertainties in modal identification.

## ACKNOWLEDGEMENTS

The research presented in this paper has been carried out within the framework of the project "Structural Health Monitoring of bridges based on heterogeneous data enriched with physical simulation", funded by the Research Foundation Flanders (FWO), Belgium (Grant no. 12B2K24N).

## REFERENCES

[1] Y. An, E. Chatzi, S. Sim, S. Laflamme, B. Blachowski, and J. Ou. Recent progress and future trends on damage identification methods for bridge structures. *Structural Control and Health Monitoring*, 26(10):e2416, 2019.

[2] D. Anastasopoulos and E. P. B. Reynders. Dynamic strain-based monitoring of a historic Vierendeel truss bridge under changing environmental and support conditions. *Journal of Civil Structural Health Monitoring*, 2024. doi: https://doi.org/10.1007/s13349-024-00888-5.

[3] Z. Zhou, S. Xue, C. Wan, and B. Wu. Optimal sensor placement and Bi-type response reconstruction for structural health monitoring using long-gauge fbg strain sensing network. *Structures*, 63 (106406), 2024.

[4] C. Leyder, V. Dertimanis, A. Frangi, E. Chatzi, and G. Lombaert. Optimal sensor placement methods and metrics - Comparison and implementation on a timber frame structure. *Structure and Infrastructure Engineering*, 14(7):997–1010, 2018.

[5] S. H. Kim and C. Cho. Effective independence in optimal sensor placement associated with general fisher information involving full error covariance matrix. *Mechanical Systems and Signal Processing*, 212(111263), 2024.

[6] P. Van Bogaert and B. De Pauw. Load-carrying capacity of Vierendeel bridges in Mechelen. *ce/papers*, 6(5):416–421, 2023.

[7] C. Papadimitriou and G. Lombaert. The effect of prediction error correlation on optimal sensor placement in structural dynamics. *Mechanical Systems and Signal Processing*, 28:105–127, 2012.

[8] S. François, M. Schevenels, D. Dooms, J. Jansen, J. Wambacq, G. Lombaert, G. Degrande, and G. De Roeck. Stabil: an educational Matlab toolbox for static and dynamic structural analysis. *Computer Applications in Engineering Education*, 29(5):1372–1389, 2021.